

Quantifying leaf trait covariation and its controls across climates and biomes

Article

Accepted Version

Yang, Y., Wang, H., Harrison, S. P. ORCID:
<https://orcid.org/0000-0001-5687-1903>, Prentice, I. C., Wright,
I. J., Peng, C. and Lin, G. (2019) Quantifying leaf trait
covariation and its controls across climates and biomes. *New
Phytologist*, 221 (1). pp. 155-168. ISSN 1469-8137 doi:
10.1111/nph.15422 Available at
<https://centaur.reading.ac.uk/78149/>

It is advisable to refer to the publisher's version if you intend to cite from the work. See [Guidance on citing](#).

To link to this article DOI: <http://dx.doi.org/10.1111/nph.15422>

Publisher: Wiley

All outputs in CentAUR are protected by Intellectual Property Rights law, including copyright law. Copyright and IPR is retained by the creators or other copyright holders. Terms and conditions for use of this material are defined in the [End User Agreement](#).

www.reading.ac.uk/centaur

CentAUR

Central Archive at the University of Reading

Reading's research outputs online

Quantifying leaf trait covariation and its controls across climates and biomes

Yanzheng Yang^{1,2,3,*}, Han Wang^{1,3}, Sandy P. Harrison^{3,4}, I. Colin Prentice^{1,3,5,6}, Ian J. Wright⁶, Changhui Peng^{3,7,*} and Guanghui Lin^{1,8,*}

¹Ministry of Education Key Laboratory for Earth System Modeling, Department of Earth System Science, Tsinghua University, Beijing 100084, China.

²Joint Center for Global Change Studies (JCGCS), Beijing 100875, China

³Center for Ecological Forecasting and Global Change, College of Forestry, Northwest A&F University, Yangling, Shaanxi 712100, China

⁴School of Archaeology, Geography and Environmental Sciences (SAGES), University of Reading, Reading, UK

⁵AXA Chair of Biosphere and Climate Impacts, Imperial College London, Department of Life Sciences, Silwood Park Campus, Buckhurst Road, Ascot SL5 7PY, UK

⁶Department of Biological Sciences, Macquarie University, North Ryde, NSW 2109, Australia

⁷Department of Biological Sciences, Institute of Environmental Sciences, University of Quebec at Montreal, C.P. 8888, Succ. Centre-Ville, Montréal H3C 3P8, QC, Canada

⁸Key Laboratory of Stable Isotope and Gulf Ecology, Graduate School at Shenzhen, Tsinghua University, Shenzhen, Guangdong 518055, China

Revised version for *New Phytologist*

(*Authors for correspondence: tel +86(10)62797230; email yanzheng148@163.com (Y.Y.); tel +86(10)62797230; email lingh@tsinghua.edu.cn (G.L.); tel +86(29)87080608; email cpeng86@yahoo.com (C.P.))

29 **Summary**

- 30 • Plant functional ecology requires the quantification of trait variation and its
31 controls. Field measurements on 483 species at 48 sites across China were used to
32 analyse variation in leaf traits, and assess their predictability.
- 33 • Principal components analysis (PCA) was used to characterize trait variation,
34 redundancy analysis (RDA) to reveal climate effects, and RDA with variance
35 partitioning to estimate separate and overlapping effects of site, climate, life-form
36 and family membership.
- 37 • Four orthogonal dimensions of total trait variation were identified: leaf area (LA),
38 internal-to-ambient CO₂ ratio (χ), leaf economics spectrum traits (specific leaf
39 area (SLA) *versus* leaf dry matter content (LDMC) and nitrogen per area (N_{area})),
40 and photosynthetic capacities (V_{cmax} , J_{max} at 25°C). LA and χ covaried with
41 moisture index. Site, climate, life form and family together explained 70% of trait
42 variance. Families accounted for 17%, and climate and families together 29%
43 LDMC and SLA showed the largest family effects. Independent life-form effects
44 were small.
- 45 • Climate influences trait variation in part by selection for different life forms and
46 families. Trait values derived from climate data via RDA showed substantial
47 predictive power for trait values in the available global data sets. Systematic trait
48 data collection across all climates and biomes is still necessary.

49
50 **Key words:** climate, leaf economics spectrum, multivariate analysis, photosynthetic
51 capacity, phylogeny, plant functional traits.

52

53 **Introduction**

54 Functional traits generally do not vary independently, but show broadly predictable
55 patterns of covariation (Armbruster *et al.*, 1996; Watson *et al.*, 2016). The covariation
56 of traits may mean that traits share genetic controls, or that they have related roles in
57 community assembly and function (Wright *et al.*, 2007; Fajardo *et al.*, 2011).
58 Quantifying the covariation of vegetative traits and their controls is important for an
59 understanding of how plants drive ecosystem processes and determine the responses
60 of ecosystems to environmental change (Wright *et al.*, 2007; Shipley *et al.*, 2011;
61 Swenson 2013; van Bodegom *et al.*, 2014; Kong *et al.*, 2014; Kraft *et al.*, 2015).
62 Although a number of large-scale studies have quantified both trait covariation (e.g.
63 Wright *et al.*, 2004; Armbruster *et al.*, 2014; Peiman & Robinson, 2017) and
64 trait-environment relationships,(e.g. Wright *et al.*, 2005; Harrison *et al.*, 2010; Liu *et*
65 *al.*, 2012; Maire *et al.*, 2015; Meng *et al.*, 2015), a number of general issues await
66 resolution. These include:

67 (1) The dimensionality of trait space – that is, the extent to which combinations of
68 different traits are independent, *versus* belonging to a set of covarying traits as
69 exemplified by the leaf economics spectrum (LES) (Wright *et al.*, 2004, 2005). The
70 intrinsic dimensionality of traits is the minimum number of independent axes that
71 adequately describe the functional variation among species, and is therefore an
72 important quantity in comparative ecology (Laughlin, 2014).

73 (2) The extent to which trait variation is determined by climate, versus the
74 co-existence of multiple trait values in the same climate (Adler *et al.*, 2013;
75 Valladares *et al.*, 2015).

76 (3) The extent to which trait variation and trait-environment correlations are linked to
77 ‘hard-wired’ physiognomic (life-form) and/or phylogenetic differences among species,
78 and the role of environment in selecting among life forms and clades (Díaz *et al.*,
79 2013; Ackerly, 2009; Donovan *et al.*, 2014).

The dimensionality question has received attention in plant functional ecology partly because of the universal nature of the LES, which is considered as the outcome of a tradeoff between resource acquisition and conservation – representing different general strategies for existence, rather than adaptations to environment (Wright *et al.*, 2007; Kong *et al.*, 2014; Reich, 2014). An early synthesis led to a proposal for four trait dimensions indexed by leaf mass per area and lifespan (i.e. the LES), seed mass and seed output, leaf and twig size, and plant height (Westoby *et al.*, 2002). Wright *et al.* (2007) found three independent trait dimensions represented by specific leaf area (SLA), seed/fruit size and leaf size in seven neotropical forests. The most extensive study (in terms of the number of species considered) to date was by Díaz *et al.* (2016), who showed that variation among species in height, stem specific density, leaf mass per area, seed mass, and nitrogen per unit mass (N_{mass}) could be reduced to two dimensions, the first indexing plant size, the second the LES. However, these various studies have considered only a limited set of traits or combined information from disparate sources, and did not attempt to quantify the climatic or phylogenetic controls on traits.

In this paper, we examine a suite of leaf traits, using co-located measurements to quantify the contributions of climate, site, life form and phylogeny to trait variation at a large geographic scale. Our analysis is based on an extensive data set (Wang *et al.*, 2018), containing information on multiple leaf traits from different regions of China. We focused on seven leaf traits that together capture many functions of plants (Table S1). The traits considered include four commonly measured traits: leaf area (LA), specific leaf area (SLA), leaf dry matter content (LDMC) and leaf nitrogen per unit area (N_{area}), and also three traits that determine photosynthetic rates: maximum carboxylation rate (V_{cmax}) and maximum electron transport rate (J_{max}), derived from gas exchange measurements in the field, and the ratio of intercellular to ambient carbon dioxide (CO_2) concentration (often denoted as $c_i:c_a$ but called χ here following Prentice *et al.*, 2014) derived from leaf stable carbon isotope ($\delta^{13}\text{C}$) measurements.

We used multivariate analysis to quantify the dimensionality of variation in this set of traits, and the nature and dimensionality of trait-climate relationships. We used variance partitioning to attribute trait variations (for all traits, and each trait separately) to differences among sites, climate variations across sites, and distinctions among life forms and plant families. We finally applied the trait-climate relationships derived from the data set to various global datasets for specific traits, in order to assess their generality and potential wider application.

Materials and methods

Dataset description

The data are derived from the China Plant Trait Database (Wang *et al.*, 2018), which contains information on morphological, physical, chemical and photosynthetic traits from 122 sites and provides information on more than 1215 species. The database was designed to provide comprehensive sampling of different vegetation types and climates. It employs a standardized taxonomy and includes information on life form, plant family, site location, elevation, and climate. LA, SLA, N_{area} , LDMC and leaf $\delta^{13}C$ data from multiple species were available at 48 sites, including 483 species altogether, distributed through the eastern half of China (Fig. 1a, Table S2). The sites from northeastern China are distributed along an aridity gradient (Prentice *et al.*, 2011), including steppes, grasslands and temperate deciduous broadleaf forests. The sites from southwestern China represent tropical and subtropical evergreen broadleaf forests, and tropical dry woodlands. Temperate deciduous forests in central China and boreal forests in the far north of China were also included. Collectively these data cover the principal climatic and vegetation zones of the region (Fig. 1b). At each site, a stratified sampling strategy ensured that measurements were available for the main species in each canopy stratum, including up to 25 species of trees. Species were classified by life form as trees, small trees, lianas, shrubs, forbs and graminoids. Bamboos, herbaceous climbers, geophytes and pteridophytes were present only in

small numbers in the dataset and were not included in our analysis. Fig. S1 shows frequency distributions of each trait within each life form for forest and non-forest sites. Table S3 lists the total number of samples in each class.

Details of trait measurement methods can be found in Wang *et al.* (2018). LA, SLA, N_{area} and LDMC were measured on samples collected in the field following standard protocols (Cornelissen *et al.*, 2003). LA was taken as the projected area of a leaf, or leaflet in the case of compound leaves. V_{cmax} was calculated from the light-saturated rate of net CO₂ fixation at ambient CO₂ (A_{sat}) using the so-called one-point method, which provides a rapid and effective alternative to the measurement of a full A-c_i curve (De Kauwe *et al.*, 2016). J_{max} was calculated from the light-saturated rate of net CO₂ fixation at high CO₂ (A_{max}). Both V_{cmax} and J_{max} were adjusted to a standard temperature of 25°C using the methods proposed by Niinemets *et al.* (2014). The adjusted values are called V_{cmax25} and J_{max25} . Leaf $\delta^{13}C$ measurements were converted to ^{13}C discrimination and thence to χ , eliminating the effects of latitude and sampling year as described in Cornwell *et al.* (2017):

$$\delta^{13}C_{air,1992} = a * \left(\sin \left(\varphi * \frac{\pi}{180} \right) \right)^2 + \sin \left(\varphi * \frac{\pi}{180} \right) - c \quad (1)$$

where φ is latitude and a , b and c are parameters estimated by regression with values $a = 0.0819$, $b = 0.0983$ and $c = 7.7521$ (Cornwell *et al.*, 2017), and

$$\delta^{13}C_{air} = \delta^{13}C_{air,1992} + g(y - 1992) \quad (2)$$

where y is the sampling year and $g = -0.0467$, and

$$\chi = (\delta^{13}C_{air} - \delta^{13}C_{plant} - a') / (b' - a') \quad (3)$$

where a' is the discrimination against $^{13}CO_2$ during diffusion through stomata (4.4‰) and b' is the discrimination against $^{13}CO_2$ during carboxylation (27‰) (Farquhar *et al.*, 1982). Cernusak *et al.* (2013) showed that about 80% of the variation in instantaneous

gas exchange measurements of χ could be accounted for by a linear relationship to $\delta^{13}\text{C}$, supporting the use of equation (3). Estimates of χ based on $\delta^{13}\text{C}$ measurements are used here, however, because they reflect longer-term growth conditions better.

Three bioclimate variables adequately represent the controls on vegetation structure and composition across China (Wang *et al.*, 2013). These are the accumulated photosynthetically active radiation during the thermal growing season (PAR_0), defined as the period when daily temperature is above 0°C ; the daily mean temperature during the thermal growing season (mGDD_0); and the ratio of mean annual precipitation to annual equilibrium evapotranspiration (moisture index, MI), calculated using SPLASH (Davis *et al.*, 2017). The primary data for the calculation of these bioclimatic variables were derived from 1814 meteorological stations (740 stations with data from 1971 to 2000, the rest from 1981 to 1990), interpolated to 1 km resolution with elevation as a covariate using ANUSPLIN V4.37 (Hutchinson 2007).

Gap filling

Photosynthetic measurements were only available for 14 sites in the China Plant Trait Database; however, these sites comprise 53% of the species represented in the data set. Photosynthetic measurements were not available for the temperate forests of Changbai Mountain, and the Inner Mongolia grasslands. In order to allow multivariate analysis of a larger data set, V_{cmax} values for species at these sites were gap-filled using a back-propagation neural network using LMA, N_{area} , LA, χ and moisture index (MI) as predictors (`newff` function in Matlab 2010a). The neural network is a machine learning technique that often provides better performance than conventional statistical methods for this type of application (Paruelo *et al.*, 1997; Papale *et al.*, 2003; Moffat *et al.*, 2010). The data were divided into two parts: a calibration data set used to determine the weights in the neural network (75% of data points), and a validation data set used to assess the network performance (25% of data points). The method achieved an acceptable accuracy with $R^2 = 0.49$ between observed and predicted

values for the calibration data set and 0.50 for the validation data set. J_{\max} values were then estimated from V_{\max} values using a linear regression fitted to data from all sites where both A_{sat} and A_{\max} were measured. The regression equation used for gap-filling is $\ln J_{\max,25} = -0.0221 \text{ mGDD}_0 + 0.7329 \ln V_{\max,25} + 2.0362$ ($R^2 = 0.75$, $P < 0.01$).

Multivariate analysis and variance partitioning

Principal components analysis (PCA) and *redundancy analysis* (RDA) are powerful multivariate analysis techniques with many ecological applications (White *et al.*, 2005; Maire *et al.*, 2015; Scheibe *et al.*, 2015). As a dimensionality reduction technique, PCA projects a set of data on correlated variables on to a series of composite, uncorrelated variables called principal components (James *et al.*, 1990). In RDA, these variables are chosen to maximize the extent of their correlation with a set of predictor variables (Borcard *et al.*, 1992) and are therefore described as “constrained” axes of variation. RDA also extracts further “unconstrained” axes, which are the principal components of the variation that remains after the fitted effects of the predictor variables have been removed. Here, PCA is used to analyse trait covariation; RDA is used to analyse the relationships of trait variation to climate variables; and the unconstrained axes of RDA are used to characterize the residual (within-site) variation in traits. These analyses were performed using the *vegan* package in R (Oksanen *et al.*, 2017). LA was square-root transformed before analysis to yield a linear measure of leaf size. χ was logit-transformed ($\text{logit } \chi = \ln [\chi/(1 - \chi)]$). All other traits (including $\sqrt{\text{LA}}$) were natural log-transformed. All traits were thus converted to dimensionless quantities in the range $(-\infty, \infty)$, allowing PCA and RDA to be carried out using the covariance matrix among traits with no need for further standardization. Each trait thereby has its ‘natural’ weight in the analysis. For log-transformed variables, this treatment implies that a trait with, say, 10-fold variation has twice the weight of a trait with 5-fold variation. The weight can be quantified by the standard deviation of the transformed variables ($\ln \sqrt{\text{LA}}$: 1.17, $\ln \text{SLA}$: 0.50, $\ln \text{LDMC}$: 0.38, $\ln N_{\text{area}}$: 0.59, \ln

V_{cmax25} : 0.58, $\ln J_{\text{max25}}$: 0.48, logit χ : 1.37; see also Table 3). PCA and RDA were repeated using only the species-site combinations for which actual (as opposed to gap-filled) photosynthetic trait data were available (Figs S2-S4, Tables S4-S5).

Variation partitioning quantifies the amount of variation in a predicted quantity (in multiple regression) or set of quantities (in RDA) that can be explained by different groups of predictors (Legendre & Legendre, 2012). We used the Legendre method (Legendre & Anderson, 1999; Peres-Neto *et al.*, 2006; Meng *et al.*, 2015), which explicitly accounts for correlations between groups by distinguishing unique and overlapping contributions from each group. The results are most conveniently displayed as Venn diagrams. The method was used here with RDA to assign trait variation to components linked to climate, sites, life forms, families, and the intersections of these controls.

Trait prediction

We evaluated the predictive power of the fitted trait-climate relationships in the RDA analysis, first on the data set as a whole and then using a cross-validation approach (Picard & Cook, 1984; Kohavi 1995). We performed five iterations, in which 80% of the data was used for training and 20% retained for validation. The average root-mean-squared error (RMSE) across all five trials provides the final measure of goodness-of-fit.

The general predictive power of the trait-climate relationships was then tested using four independent global trait data sets: leaf economics traits (SLA, LDMC, N_{area}) from Wright *et al.* (2004); $\sqrt{\text{LA}}$ from Wright *et al.* (2017); photosynthetic traits (V_{cmax25} , J_{max25}) from De Kauwe *et al.* (2016), including data from Bahar *et al.* (2017); and χ from Cornwell *et al.* (2017) (Table S6). Each of these data sets provides geolocated site-based measurements across continents, vegetation types and climates (Figure S5). We derived climate variables for each site from the nearest 10-minute grid cell in the

CRU 2.0 dataset (New *et al.* 2002), which provides long-term monthly means of temperature, precipitation, and sunshine duration for the standard period 1961-1990. PAR₀, mGDD₀, and MI were calculated in the same way as for the sites in China, using SPLASH to calculate MI (Davis *et al.*, 2017).

We screened out measurements from sites in the global data sets where MI > 1.4 or mGDD₀ < 10 because these are beyond the limits of the climates sampled in China. Some of the $\delta^{13}\text{C}$ measurements in Cornwell *et al.* (2017) are < -30‰. We assume that these reflect incomplete mixing of CO₂ between the free atmosphere and the forest understorey. We excluded these measurements. The number of sites and individual measurements from each global data set used to test the climate-trait predictions is shown in Table S6. Trait values at each global site were directly predicted from climate inputs, using the RDA model previously derived from the data in China. Ordinary least-squares regression was used to compare observed (y) with predicted (x) trait values.

Results

Four dimensions of trait variation

PCA of traits from all species and sampling sites revealed four independent axes of trait variation (Fig. 2, Table 1). The first four principal components together account for 95% of total trait variation. The first two axes are dominated by LA and χ , orthogonal to one another. These two axes together account for 79% of total trait variation: this large fraction draws attention to the large span of variability in these traits, especially leaf area. The third axis, accounting for 11% of total trait variation, primarily represents the LES, with SLA opposed to N_{area} and LDMC. The plot of axis 3 against axis 4, which accounts for 6% of total trait variation, shows that V_{cmax} and J_{max} vary closely together, but orthogonally to the LES.

Analysis based on sites with complete data only (Fig. S2, Table S4) shows that the first four principal components have similar explanatory power to the main analysis (93%) and, although the axes are rotated with respect to the axes derived from the larger data set, they show the same four dimensions of variation with LA, LES, photosynthetic capacity and χ varying independently of one another. The patterns of trait covariation can also be seen by examining the matrix of pairwise correlations between traits (Fig. S6). The differences between Fig. S6(a) based on the gap-filled data set, and Fig. S6(b) based on sites with complete data, show the (slight) effect of gap-filling. V_{cmax} and J_{max} are highly correlated (0.84) before gap filling. The largest difference is that the negative correlations of both V_{cmax} and J_{max} with leaf area *increase* due to the gap filling. This evidently does not contradict our inference from PCA on the gap-filled data set, i.e. that photosynthetic capacities are largely uncorrelated with the other traits.

Trait variation related to climate

The three bioclimatic variables together account for 37% of trait variation (Table 2). Three successive RDA axes (Fig. 3, Table 2) describe the patterns of trait variation with climate, and show that the between-site patterns of trait covariation imposed by climatic gradients differ from those found in the data set as a whole. The first RDA axis is overwhelmingly dominant, and is related to the gradient of MI from desert-steppe to moist forests. LA and χ vary together along this gradient, with both large leaves and large χ characteristic of wetter environments. The second RDA axis accounts for 2% of trait variation, and is related to the covariation of mean growing-season temperature and total growing-season light availability along the latitudinal gradient from the boreal zone to the tropics. Trait variation on this axis resembles the LES: warmer, higher irradiance climates are characterized by plants with lower SLA, higher LDMC and higher N_{area} . The third RDA axis accounts for only 0.4% of trait variation. Analysis based on sites with complete data only (Fig. S3, Table S5) shows the same patterns.

Residual trait variation, unrelated to climate

The unconstrained axes (or residual principal components) calculated by RDA after climatic differences among sites have been accounted for (Fig. 4, Table 2) provide insight into trait variation that is expressed within sites and across all climates. The patterns of this residual variation, as shown by the first four unconstrained axes, are similar to the patterns shown by the principal components of the whole data set (Fig. 2, Table 1), with evidence for four independent dimensions of variation associated with successive components dominated by χ , LA, LES traits and photosynthetic capacities, respectively. Analysis based on sites with complete data only (Fig. S4, Table S5) shows the same four dimensions.

The same general patterns of non-climate-related trait covariation are also clear on inspection of the partial correlations among transformed trait values, after the effects of climatic predictors have been removed (Fig. 5). Deeper colours in Fig. 5 indicate larger absolute magnitudes of correlation. The traits can be seen to fall into four blocks: one comprising V_{cmax} and J_{max} (positively correlated), one comprising the traits that contribute to the LES (SLA negatively correlated with LDMC and N_{area}), χ , and LA. While χ shows almost no correlation with any of the other traits, LA is weakly negatively correlated with V_{cmax} and J_{max} (Fig. 5), as is SLA.

Multiple controls of trait variation

Venn diagrams (Fig. 6) summarize the percentage contributions of climate, site, life form and family (including intersecting contributions) to total trait variation, and to variation in each separate trait. The intersection regions represent trait variation that cannot be unambiguously attributed to one control or another, because of correlations among the controls. For example, substantial intersections between climate and family occur because these controls are not independent: different families are selected for in different climates. Anomalously large values are highlighted in bold in Fig. 6 and one

anomalously small value indicated by italics. No values are shown for climate independently of site, because differences in climate are determined by site locations. Table 3 also shows the total percentage of variance associated with each control (including intersections with other controls).

Considering the variation among all traits together (Fig. 6), climate, site, family and life form jointly account for 70% of total trait variance. The most important features of the partitioning are (1) the joint effect of climate with family (23%), which is the dominant driver of trait variation in this dataset; (2) the substantial fraction of variance due to family alone (17%), independent of climate or life form; and (3) the fact that most of the total variance associated with life form (16%) is also linked to climate (8%). There is some additional effect of climate independent of family (8%); and some effect of site independent of climate (12%), which is presumably related to edaphic or microclimatic factors.

The partitioning of trait variance for individual traits (Fig. 6) generally resembles that for all traits. However, 48% of total trait variation in LDMC is linked to family, and 41% linked to family independent of other controls. Only 4% of the variation in LDMC is linked to climate, and none to climate and family together. For SLA, 41% of total trait variation is linked to family (with 14% linked to family and life form together independent of other controls); 15% is linked to climate, but only 4% to climate and family together. These anomalies indicate a particularly strong phylogenetic component to variation in LDMC and, to a lesser extent, SLA. The unexplained variation is greater for V_{cmax25} (47%) and J_{max25} (41%) than for the other traits.

After climate, site and family effects have been accounted for, the remaining (independent) contribution of life form to trait variation is small. The total life-form contribution is < 10% for all traits except LA and χ , and the unique contribution of life form independent of all other controls is very slight, < 2.5% for all traits. Forbs and

graminoids show different ranges of trait values in forest and non-forest vegetation (Fig. S1). Specifically, SLA and LDMC of forbs and graminoids decrease between forests and non-forests while N_{area} , V_{cmax} and J_{max} increase. That is, for all these traits, life forms occupying the understorey in forest vegetation become more ‘tree-like’ in non-forest vegetation, suggesting that these traits are more determined by the light environment than by any intrinsic difference among life forms.

Worldwide prediction of traits based on the observed climate-trait relationships

The RDA analyses show that climate (including indirect effects mediated by selection for life forms and families) is the major determinant of trait variation for most of the traits examined, except for LDMC and SLA, which show a substantial independent phylogenetic component. This generalization is supported by predictions of the mean site values for each trait (Fig S7). At species level, the adjusted R^2 between observed and predicted values for LDMC is only 0.08, and for SLA 0.16 (Table S7), while the relationship is better for other traits – from 0.24 for $V_{\text{cmax}25}$ to 0.52 for $\sqrt{\text{LA}}$. The average adjusted R^2 across traits is 0.28. Partitioning the data into woody and non-woody components has little impact on the quality of the prediction for most traits, but prediction of LDMC and SLA is better for non-woody than woody species (Table S7). Although predictability is imperfect, because of the (demonstrated) influence of non-climatic factors on all of the traits, these analyses nonetheless show that it is possible to predict all four dimensions of trait variation, to first order, from climate.

The prediction of trait values in global data sets provides a more stringent test of the universality of the derived climate-trait relationships (Fig. 7, Table 4). At site level, the lowest adjusted R^2 value between observed and predicted trait values is again for LDMC (0.01), but for SLA it is 0.31. For other traits, adjusted R^2 ranged from 0.25 (J_{max}) to 0.34 ($\sqrt{\text{LA}}$). The average across traits is 0.31, excluding LDMC. The observed values for $\ln V_{\text{cmax}25}$ tend to be higher than the predicted values, whereas the observed values of $\ln \text{SLA}$ tend to be lower than the predicted values (Fig. 7).

However the regression slopes for these traits are not significantly different from unity (Table 4). The OLS regression slopes for $\ln \sqrt{LA}$, $J_{\max 25}$ and $\ln \chi$ are in the range from 0.48 to 1. RMSE values (Table 4) are larger in the global comparison than in the calibration set for $\ln \sqrt{LA}$ and SLA; but closely similar for N_{area} , $V_{\text{cmax}25}$ and $J_{\max 25}$, and χ . The average RMSE across traits excluding LDMC is slightly less in the global comparison (0.42) than in the calibration set (0.61).

Discussion

The ecological significance of leaf-trait dimensions

The four dimensions of total leaf-trait variation reported here indicate the existence of independent variation among species in LA, χ , photosynthetic capacity, and the LES. The RDA based on climate shows a smaller dimensionality, with most of the variation concentrated on a single axis from wet to dry environments. LA is both expected and observed to increase with plant-available moisture, due to energy-balance constraints (Wright *et al.*, 2017). χ is both expected and observed to increase with atmospheric moisture according to the least-cost hypothesis (Prentice *et al.*, 2014). These hydroclimatic controls on both LA and χ are presumed to be the cause of (a) the dominance of a single dimension of trait-environment relationships across the region, related to moisture/aridity, and (b) the observed close covariation of LA and χ between sites along the aridity gradient – contrasting with their independence in the data as a whole. Analysis of the residual (non-climatic) component of trait variation however shows, once again, four independent dimensions, with a pattern closely similar to that shown in total leaf-trait variation, and orthogonal variation of LA and χ .

Multivariate analysis confirms the universal nature of the LES, as indexed here by SLA, LDMC (which tends to be high when SLA is low), and N_{area} . Unlike N_{mass} (N concentration per unit mass), N_{area} increases with *decreasing* SLA because the structural component of leaf N increases in proportion to LMA (see e.g. Onoda *et al.*,

2004, 2017; Wright *et al.*, 2005; Osnas *et al.*, 2013; Dong *et al.*, 2017a). The LES is identified in the PCA, and in the residual trait variation after consideration of climate effects in RDA. However, it also appears in the climatically constrained RDA as a second-order pattern correlated with the latitudinal gradient. In other words, there is a shift in the average position of species along the LES (towards lower SLA) with increasing growing-season length and warmth, although this shift accounts only for a small proportion (2%) of total trait variance. The LES reflects the inescapable linkage between high construction costs and long payback times of leaves with low SLA (Kikuzawa, 1991; Reich *et al.*, 1997; McMurtrie & Dewar, 2011; Funk & Cornwell, 2013). The shift towards lower-SLA leaves in warmer climates is primarily due to the shift of dominance from deciduous to evergreen woody plants. The increase in growing-season length (towards a year-round growing season in the tropics) favours longer-lived evergreen leaves with lower SLA in warmer climates, as shown here and in other studies.

Both the gap-filled data set and the non-gap-filled subset show that the two photosynthetic capacities (V_{cmax} and J_{max}) covary closely (Fig. S6), as is expected from the co-ordination hypothesis – which predicts that leaves should not possess excess capacity in either carboxylation or electron transport, as photosynthesis depends on both (Chen *et al.*, 1993; Maire *et al.*, 2012). However both traits show substantial variation within sites. When V_{cmax} and J_{max} were entered into the analysis after adjustment to local growth temperature, as opposed to 25°C, the results were very similar (not shown). Opposite trends of variation in V_{cmax} and J_{max} are shown only in the (minor) third axis of the RDA, accounting for 0.4% of total trait variance and driven by differences among sites in summer temperature that are independent of the latitudinal gradient. This pattern is consistent with expectations, as a decline in the $J_{\text{max}}:V_{\text{cmax}}$ ratio with increasing temperature has been shown experimentally (Kattge & Knorr, 2007) and predicted theoretically (Wang *et al.*, 2017a). The decline is larger

when the two photosynthetic capacities are estimated at prevailing growth temperature, but persists when they are adjusted to 25°C.

Contributions to leaf trait variation

The variance partitioning results presented here demonstrate that family and climate effects (except for LDMC and SLA) overlap considerably. In other words, a substantial part of trait variation with climate is due to families replacing one another along environmental gradients. After family, climate and site effects have been taken into account, independent life-form effects become unimportant. Thus, to first order, the principal controls on trait variation in this data set are family identity, climate, and climatic selection among families. Additional effects of site (independent of climate) could in principle be due to microclimatic and/or edaphic differences among sites, which have not been investigated. LDMC and to a lesser extent SLA show stronger family effects than other traits, while the effects of climate on these traits appear to be largely independent of family identity.

Implications for vegetation modelling

Vegetation models based on continuous variation in trait space sample ‘plants’ from a continuum of trait values (e.g. Scheiter *et al.*, 2013; Fyllas *et al.*, 2014). This approach requires specifying which traits can vary; by how much; and the extent to which different traits covary, in other words, the effective dimensionality of trait space. Our analyses of leaf traits, including traits derived from stable isotope and gas exchange measurements, indicate that at least four independent dimensions of trait variation need to be considered; that realistic modelling of functional diversity must allow for within-site variation in each of these dimensions; and that environmental differences force patterns of trait covariation across sites that can be different from patterns observed within sites.

With the exception of LDMC, which shows a particularly strong phylogenetic component, the trait-environment relationships found here should be amenable to process-based modelling. The energy balance implications of leaf size (Michaletz *et al.*, 2016; Dong *et al.*, 2017b; Wright *et al.*, 2017) mean that this trait is crucial for survival, particularly in cold climates or in hot, dry climates. As the biophysical controls of leaf size are relatively well understood, it should be straightforward to build energy-balance constraints on leaf size into trait-based models. Shifts in the LES along environmental gradients could also be modelled, given the well-established relationship of leaf longevity and SLA (Wright *et al.*, 2004) and the experimentally determined variations of SLA with environmental factors (Poorter *et al.*, 2009). The distribution of SLA within communities could be represented by a pattern of covariation in leaf longevity, SLA, LDMC and the structural component of N_{area} , as shown here and in other studies.

The co-ordination hypothesis predicts both V_{cmax} and the ratio of J_{max} to V_{cmax} , including the observed dependence of both quantities on growth temperature (Wang *et al.*, 2017b). Large-scale patterns in V_{cmax} and the metabolic component of N_{area} can be predicted theoretically (Dong *et al.*, 2017a). The co-ordination hypothesis also predicts the observed seasonal acclimation of V_{cmax} and J_{max} (Togashi *et al.*, 2018). Thus, at the level of community mean values, it seems likely that V_{cmax} can be successfully modelled as a function of environment (Ali *et al.*, 2016). A temperature-dependent ratio of J_{max} to V_{cmax} would then allow prediction of J_{max} .

The CO₂ drawdown from air to leaf, indexed by χ , is predicted by most vegetation models by simultaneous solution of the FvCB equations to predict assimilation rate as a function of leaf-internal CO₂ (c_i) and the diffusion equation to predict c_i as a function of ambient CO₂ (c_a), stomatal conductance and assimilation rate (Farquhar *et al.*, 1980). Theoretically and empirically well-founded relationships between χ and

environmental variables (Wang *et al.*, 2017b) provide an alternative way to model χ directly as a function of environment, and thus to predict assimilation rates more straightforwardly than in many current models.

Challenges and future directions

This analysis illustrates the power of large trait data sets spanning a large range of climates, and including measurements from multiple co-existing species at each field site, to reveal general patterns. It also shows the utility of multivariate analysis to summarize patterns, and variance partitioning to attribute trait variability to different (and sometimes intersecting) causes. But despite the availability of large plant-trait data compilations (e.g. Kattge *et al.*, 2011), the number of sites that include all of any specified set of plant traits is often disappointingly small – because different research groups typically collect data on different sets of traits. There remains a need for more extensive trait data collection including photosynthetic traits and isotopic measurements in addition to conventional leaf traits, and for such data collection to extend to the full range of the world's climates. There has been a limited amount of comparative work, for example, on photosynthetic traits, which are essential for all process-based vegetation modelling. Moreover, compared to leaf traits, there is a paucity of data on other field-measurable traits (notably stem hydraulic properties) that may be equally important for plant functional ecology. As is well illustrated by the global data sets that we used to test the predictive capacity of trait-climate relationships, the site- and/or species-metadata available are often limited. There remains a need for extensive, targeted collection and analysis of plant trait data, including co-located morphological, gas-exchange and isotopic measurements, and spanning the world's major environmental and floristic gradients.

501 **Acknowledgments**

502 This research has been by supported by High-end Foreign Expert Programmes of
503 China (GDW20156100290, GDW20166100147) (ICP and SPH), the National Natural
504 Science Foundation of China (41701051, 31600388) (YY and HW), the National Basic
505 Research Program of China (2013CB956600) (GL and CP), the Fundamental Research
506 Funds for the Central Universities (YY), the QianRen Program, and the Natural
507 Sciences and Engineering Research Council of Canada (NSERC) Discover Grant (CP).
508 SPH acknowledges support from the ERC-funded project GC2.0 (Global Change 2.0:
509 Unlocking the past for a clearer future, grant number 694481). This research
510 contributes to the AXA Chair Programme in Biosphere and Climate Impacts and the
511 Imperial College initiative on Grand Challenges in Ecosystems and the Environment
512 (ICP). We thank O. Atkin, K. Crous, T. Domingues, D. Ellsworth, H. Togashi, Ü.
513 Niinemets and L. Weerasinghe for providing the photosynthesis data ($V_{\text{cmax}25}$, $J_{\text{max}25}$)
514 used in the validation.

515 **Author contributions**

516 YY, HW, SPH and ICP collectively devised the analysis strategy and interpreted the
517 results. YY carried out all of the statistical analyses and wrote the first draft of the
518 manuscript. IJW provided additional advice on the analysis and interpretation of trait
519 variation patterns. All authors provided input to the final draft.

520 **References**

- 521 **Ackerly D. 2009.** Conservatism and diversification of plant functional traits:
522 evolutionary rates versus phylogenetic signal. *Proceedings of the National*
523 *Academy of Sciences* **106 (Suppl. 2)**: 19699-19706.
- 524 **Ackerly DD, Cornwell WK. 2007.** A trait-based approach to community assembly:
525 partitioning of species trait values into within- and among-community
526 components. *Ecology Letters* **10**: 135-145.
- 527 **Adler PB, Fajardo A, Kleinhesselink AR, Kraft NJ. 2013.** Trait-based tests of
528 coexistence mechanisms. *Ecology Letters* **16**: 1294-1306.
- 529 **Ali A, Xu C, Rogers A, Fisher R, Wullschlegel S, McDowell N, Massoud E, Vrugt**
530 **J, Muss J, Fisher J et al. 2016.** A global scale mechanistic model of the
531 photosynthetic capacity (LUNA V1.0). *Geoscientific Model Development* **9**:
532 587-606.
- 533 **Armbruster WS, Pélabon C, Bolstad GH, Hansen TF. 2014.** Integrated phenotypes:
534 understanding trait covariation in plants and animals. *Philosophical*
535 *Transactions of the Royal Society B: Biological Sciences* **369**: 20130245.
- 536 **Armbruster WS, Schwaegerle KE. 1996.** Causes of covariation of phenotypic traits
537 among populations. *Journal of Evolutionary Biology* **9**:261-76.
- 538 **Bahar NHA, Ishida FY, Weerasinghe LK, Guerrieri R, O'Sullivan OS, Bloomfield**
539 **KJ, Asner GP, Martin RE, Lloyd J, Malhi Y et al. 2017.** Leaf-level
540 photosynthetic capacity in lowland Amazonian and high-elevation Andean
541 tropical moist forests of Peru. *New Phytologist* **214**: 1002-1018.
- 542 **Borcard D, Legendre P, Drapeau P.1992.** Partialling out the spatial component of
543 ecological variation. *Ecology* **84**: 511-525.
- 544 **Cernusak LA, Ubierna N, Winter K, Holtum JAM, Marshall JD, Farquhar GD.**
545 **2013.** Environmental and physiological determinants of carbon isotope
546 discrimination in terrestrial plants. *New Phytologist* **200**: 950-965.

547 **Chen JL, Reynolds JF, Harley PC, Tenhunen JD. 1993.** Coordination theory of leaf
548 nitrogen distribution in a canopy. *Oecologia* **93**: 63-69.

549 **Cornwell WK, Wright I, Turner J, Maire V, Barbour M, Cernusak L, Dawson T,**
550 **Ellsworth D, Farquhar G, Griffiths H et al. 2017.** A global dataset of leaf Δ
551 ^{13}C values. 10.5281/zenodo.569501

552 **Cornelissen J, Lavorel S, Garnier E, Díaz S, Buchmann N, Gurvich D, Reich P,**
553 **Ter Steege H, Morgan H, van der Heijden M. 2003.** A handbook of
554 protocols for standardised and easy measurement of plant functional traits
555 worldwide. *Australian Journal of Botany* **51**: 335-380.

556 **De Kauwe MG, Lin YS, Wright IJ, Medlyn BE, Crous KY, Ellsworth DS, Maire V,**
557 **Prentice IC, Atkin OK, Rogers A. 2016.** A test of the 'one-point method' for
558 estimating maximum carboxylation capacity from field-measured,
559 light-saturated photosynthesis. *New Phytologist* **210**: 1130-1144.

560 **Davis TW, Prentice IC, Stocker BD, Thomas RT, Whitley RJ, Wang H, Evans BJ,**
561 **Gallego-Sala AV, Sykes MT, Cramer W. 2017.** Simple process-led
562 algorithms for simulating habitats (SPLASH v. 1.0): robust indices of radiation,
563 evapotranspiration and plant-available moisture. *Geoscientific Model*
564 *Development* **10**: 689-708.

565 **Díaz S, Purvis A, Cornelissen JH, Mace G M, Donoghue MJ, Ewers RM, Jordano**
566 **P, Pearse WD. 2013.** Functional traits, the phylogeny of function, and
567 ecosystem service vulnerability. *Ecology and evolution*, **3**: 2958-2975.

568 **Díaz S, Kattge J, Cornelissen JHC, Wright IJ, Lavorel S, Dray S, Reu B, Kleyer**
569 **M, Wirth C, Prentice IC et al. 2016.** The global spectrum of plant form and
570 function. *Nature* **529**: 167-173.

571 **Dong N, Prentice IC, Evans BJ, Caddy-Retalic S, Lowe AJ, Wright IJ. 2017a.** Leaf
572 nitrogen from first principles: field evidence for adaptive variation with climate.
573 *Biogeosciences* **14**: 481-495.

574 **Dong N, Prentice IC, Harrison SP, Song Q, Zhang YP. 2017b.** Biophysical
575 homoeostasis of leaf temperature: a neglected process for vegetation and
576 land-surface modelling. *Global Ecology and Biogeography* **9**: 998-1007.

577 **Donovan LA, Mason CM, Bowsher AW, Goolsby EW, Ishibashi CD. 2014.**
578 Ecological and evolutionary lability of plant traits affecting carbon and nutrient
579 cycling. *Journal of Ecology* **102**:302-14

580 **Fajardo A, Piper FI. 2011.** Intraspecific trait variation and covariation in a widespread
581 tree species (*Nothofagus pumilio*) in southern Chile. *New Phytologist* **189**:
582 259-71.

583 **Farquhar G, von Caemmerer S, Berry J. 1980.** A biochemical model of
584 photosynthetic CO₂ assimilation in leaves of C₃ species. *Planta* **149**: 78-90.

585 **Farquhar G, O'Leary M, Berry J. 1982.** On the relationship between carbon isotope
586 discrimination and the intercellular carbon dioxide concentration in leaves.
587 *Functional Plant Biology* **9**: 121-137.

588 **Funk JL, Cornwell WK. 2013.** Leaf traits within communities: context may affect the
589 mapping of traits to function. *Ecology* **94**: 1893-1897.

590 **Fyllas NM, Gloor E, Mercado LM, Sitch S, Quesada CA, Domingues TF,**
591 **Galbraith DR, Torre-Lezama A, Vilanova E, Ramírez-Angulo H et al.**
592 **2014.** Analysing Amazonian forest productivity using a new individual and
593 trait-based model (TFS v.1). *Geoscientific Model Development* **7**: 1251-1269.

594 **Harrison SP, Morfopoulos C, Dani KGS, Prentice IC, Arneth A, Atwell BJ,**
595 **Barkley MP, Leishman MR, Loreto F, Medlyn BE et al. 2013.** Volatile
596 isoprenoid emissions from plastid to planet. *New Phytologist* **197**: 49-57.

597 **Hutchinson, M.2007.** ANUSPLIN Version 4.37 User Guide. *The Australian National*
598 *University*.

599 **James FC, McCulloch CE. 1990.** Multivariate Analysis in Ecology and
600 Systematics:Panacea or Pandora's Box? *Annual Review of Ecology and*
601 *Systematics* **21**:129–166.

602 **Kattge J, Díaz S, Lavorel S, Prentice IC, Leadley P, Bönisch G, Garnier E,**
603 **Westoby M, Reich PB, Wright IJ et al. 2011.** TRY – a global database of
604 plant traits. *Global Change Biology* **17**: 2905-2935.

605 **Kattge J, Knorr W. 2007.** Temperature acclimation in a biochemical model of
606 photosynthesis: a reanalysis of data from 36 species. *Plant, cell & environment*,
607 **30**: 1176-1190.

608 **Kikuzawa K. 1991.** A cost-benefit analysis of leaf habit and leaf longevity of trees and
609 their geographical pattern. *American Naturalist* **138**: 1250-1263.

610 **Kohavi R. 1995.** A study of cross-validation and bootstrap for accuracy estimation and
611 model selection. *International Joint Conference on Artificial Intelligence* **14**:
612 1137-1145.

613 **Kong D, Ma C, Zhang Q, Li L, Chen X, Zeng H, Guo D. 2014.** Leading dimensions
614 in absorptive root trait variation across 96 subtropical forest species. *New*
615 *Phytologist* **203**: 863-872.

616 **Kraft NJ, Godoy O, Levine JM. 2015.** Plant functional traits and the
617 multidimensional nature of species coexistence. *Proceedings of the National*
618 *Academy of Sciences* **112**: 797-802.

619 **Laughlin DC. 2014.** Applying trait- based models to achieve functional targets for
620 theory- driven ecological restoration. *Ecology letters* **17**:771-84.

621 **Legendre P, Anderson MJ. 1999.** Distance- based redundancy analysis: testing
622 multispecies responses in multifactorial ecological experiments. *Ecological*
623 *monographs*. **69**:1-24.

624 **Legendre P, Legendre L. 2012.** *Numerical ecology, 3rd Edition*. Amsterdam,
625 Netherland: Elsevier Science.

626 **Liu X, Swenson NG, Wright SJ, Zhang L, Song K, Du Y J, Zhang JL, Mi XC, Ren**
627 **HB, Ma KP. 2012.** Covariation in Plant Functional Traits and Soil Fertility
628 within Two Species-Rich Forests. *PLOS ONE* **7**: e34767.

629 **Maire V, Martre P, Kattge J, Gastal F, Esser G, Fontaine S, Soussana JF. 2012.**
630 The coordination of leaf photosynthesis links C and N fluxes in C₃ plant species.
631 *PLoS One* **7**: e38345.

632 **Maire V, Wright IJ, Prentice IC, Batjes NH, Bhaskar R, Bodegom PM van,**
633 **Cornwell WK, Ellsworth D, Niinemets Ü, Ordonez A et al. 2015.** Global
634 effects of soil and climate on leaf photosynthetic traits and rates. *Global Ecology*
635 *and Biogeography* **24**:706-717.

636 **McMurtrie RE, Dewar RC. 2011.** Leaf-trait variation explained by the hypothesis
637 that plants maximize their canopy carbon export over the lifespan of leaves.
638 *Tree Physiology* **31**: 1007.

639 **Meng TT, Wang H, Harrison SP, Prentice IC, Ni J, Wang G. 2015.** Responses of
640 leaf traits to climatic gradients: adaptive variation versus compositional shifts.
641 *Biogeosciences* **12**: 5339-5352.

642 **Michaletz ST, Weiser MD, McDowell NG, Zhou J, Kaspari M, Helliker BR,**
643 **Enquist BJ. 2016.** The energetic and carbon economic origins of leaf
644 thermoregulation. *Nature Plants* **2**: 16129.

645 **Moffat AM, Beckstein C, Churkina G, Mund M, Heimann M. 2010.**
646 Characterization of ecosystem responses to climatic controls using artificial
647 neural networks. *Global Change Biology* **16**:2737-2749.

648 **New M, Lister D, Hulme M, Makin I. 2002.** A high-resolution data set of surface
649 climate over global land areas. *Climate research*, **21**: 1-25.

650 **Niinemets Ü, Keenan TF, Hallik L. 2014.** A worldwide analysis of within-canopy
651 variations in leaf structural, chemical and physiological traits across plant
652 functional types. *New Phytologist* **205**: 973-993.

653 **Oksanen J, Blanchet FG, Friendly M, Kindt R, Legendre P, McGlinn D, Minchin**
654 **PR, O'Hara RB, Simpson GL, Solymos P, Stevens MH, Szoecs E. 2017.**
655 *vegan: Community Ecology Package. R package Version 2.4-4.* [WWW
656 document] URL <https://github.com/vegandevs/vegan>. [accessed 1 May 2016].

657 **Onoda Y, Hikosaka K, Hirose T. 2004.** Allocation of nitrogen to cell walls decreases
658 photosynthetic nitrogen-use efficiency. *Functional Ecology* **18**: 419-425.

659 **Onoda Y, Wright IJ, Evans JR, Hikosaka K, Kitajima K, Niinemets Ü, Poorter H,**
660 **Tosens T, Westoby M. 2017.** Physiological and structural tradeoffs underlying
661 the leaf economics spectrum. *New Phytologist* **214**: 1447-1463

662 **Osnas JL, Lichstein JW, Reich PB, Pacala SW. 2013.** Global leaf trait relationships:
663 mass, area, and the leaf economics spectrum. *Science* **340**: 741-744.

664 **Papale D, Valentini R. 2003.** A new assessment of European forests carbon exchanges
665 by eddy fluxes and artificial neural network spatialization. *Global change*
666 *biology* **9**:525-535.

667 **Paruelo JM, Tomasel F. 1997.** Prediction of functional characteristics of ecosystems:
668 a comparison of Article neutral networks and regression models. *Ecological*
669 *modelling* **98**:173-186.

670 **Peiman KS, Robinson BW. 2017.** Comparative analyses of phenotypic trait
671 covariation within and among populations. *The American Naturalist* **190**:
672 451-468.

673 **Peres-Neto PR, Legendre P, Dray S, Borcard D. 2006.** Variation partitioning of
674 species data matrices: estimation and comparison of fractions. *Ecology* **87**:
675 2614-2625.

676 **Picard RR, Cook RD. 1984.** Cross-validation of regression models. *Journal of the*
677 *American Statistical Association* **79**: 575-583.

678 **Pierce S, Brusa G, Vagge I, Cerabolini, BEL. 2013.** Allocating CSR plant functional
679 types: the use of leaf economics and size traits to classify woody and
680 herbaceous vascular plants. *Functional Ecology* doi: 10.1111/1365-2435.12095

681 **Poorter H, Niinemets Ü, Poorter L, Wright IJ, Villar R. 2009.** Causes and
682 consequences of variation in leaf mass per area (LMA): a meta-analysis. *New*
683 *Phytologist* **182**: 565-588.

684 **Prentice IC, Dong N, Gleason SM, Maire V, Wright IJ. 2014.** Balancing the costs of
685 carbon gain and water transport: testing a new theoretical framework for plant
686 functional ecology. *Ecology Letters* **17**: 82-91.

687 **Prentice IC, Meng T, Wang H, Harrison SP, Ni J, Wang G. 2011.** Evidence of a
688 universal scaling relationship for leaf CO₂ drawdown along an aridity gradient.
689 *New Phytologist* **190**: 169-180.

690 **Reich PB. 2014.** The world-wide ‘fast-slow’ plant economics spectrum: a traits
691 manifesto. *Journal of Ecology* **102**: 275-301.

692 **Reich PB, Walters MB, Ellsworth DS. 1997.** From tropics to tundra: global
693 convergence in plant functioning. Proceedings of the National Academy of
694 *Sciences* **94**: 13730-13734.

695 **Scheiter S, Langan L, Higgins SI. 2013.** Next-generation dynamic global vegetation
696 models: learning from community ecology. *New Phytologist* **198**: 957-969.

697 **Scheibe A, Steffens C, Seven J, Jacob A, Hertel D, Leuschner C, Gleixner G. 2015.**
698 Effects of tree identity dominate over tree diversity on the soil microbial
699 community structure. *Soil Biology and Biochemistry* **81**: 219-227.

700 **Shipley B, Laughlin DC, Sonnier G, Otfinowski R. 2011.** A strong test of a
701 maximum entropy model of trait-based community assembly. *Ecology* **92**:
702 507-517.

703 **Swenson NG. 2013.** The assembly of tropical tree communities—the advances and
704 shortcomings of phylogenetic and functional trait analyses. *Ecograph*
705 **36**:264-76.

706 **Togashi HF, Prentice IC, Atkin OK, Macfarlane C, Prober SM, Bloomfield KJ,**
707 **Evans BJ 2018.** Thermal acclimation of leaf photosynthetic traits in an
708 evergreen woodland, consistent with the coordination hypothesis.
709 *Biogeosciences*.

710 **Valladares F, Bastias CC, Godoy O, Granda E, Escudero A. 2015.** Species
711 coexistence in a changing world. *Frontiers in Plant Science* **6**: 866.

- 712 **van Bodegom PM, Douma JC, Verheijen LM. 2014.** A fully traits-based approach to
713 modeling global vegetation distribution. *Proceedings of the National Academy*
714 *of Sciences* **111**: 13733-13738.
- 715 **Wang H, Prentice IC, Ni J. 2013.** Data-based modelling and environmental sensitivity
716 of vegetation in China. *Biogeosciences* **10**: 5817-5830.
- 717 **Wang H, Prentice IC, Cornwell WK, Keenan TF, Davis TW, Wright IJ, Evans BJ,**
718 **Peng C. 2017a.** Towards a universal model for carbon dioxide uptake by plants.
719 *Nature Plants* **3**: 734-741.
- 720 **Wang H, Prentice IC, Davis TW, Keenan TF, Wright IJ, Peng C. 2017b.**
721 Photosynthetic responses to altitude: an explanation based on optimality
722 principles. *New Phytologist* **213**: 976-982.
- 723 **Wang H, Harrison SP, Prentice IC, Yang Y, Togashi HF, Wang M, Zhou S, Bai F,**
724 **Ni J 2018.** The China Plant Trait Database: towards a comprehensive regional
725 compilation of functional traits for land plants. *Ecology* **99**: 500.
- 726 **Watson RA, Szathmáry E. 2016.** How can evolution learn? *Trends in Ecology &*
727 *Evolution* **31**:147-57.
- 728 **Westoby M, Falster DS, Moles AT, Vesk PA, Wright IJ. 2002.** Plant ecological
729 strategies: Some leading dimensions of variation between species. *Annual*
730 *Review of Ecology and Systematics* **33**: 125-159.
- 731 **White C, Tardif JC, Adkins A, Staniforth R. 2005.** Functional diversity of microbial
732 communities in the mixed boreal plain forest of central Canada. *Soil Biology &*
733 *Biochemistry* **37**: 1359-1372.
- 734 **Wright IJ, Ackerly DD, Bongers F, Harms KE, Ibarra-Manriquez G,**
735 **Martinez-Ramos M, Mazer SJ, Muller-Landau HC, Paz H, Pitman NCA et**
736 **al. 2007.** Relationships among ecologically important dimensions of plant trait
737 variation in seven neotropical forests. *Annals of Botany* **99**: 1003-1015.
- 738 **Wright IJ, Reich PB, Cornelissen JHC, Falster DS, Groom PK, Hikosaka K, Lee**
739 **W, Lusk CH, Niinemets Ü, Oleksyn J et al. 2005.** Modulation of leaf

740 economic traits and trait relationships by climate. *Global Ecology and*
741 *Biogeography* **14**: 411-421.

742 **Wright IJ, Reich PB, Westoby M, Ackerly DD, Baruch Z, Bongers F,**
743 **Cavender-Bares J, Chapin T, Cornelissen JH, Diemer M et al. 2004.** The
744 worldwide leaf economics spectrum. *Nature* **428**: 821-827.

745 **Wright IJ, Dong N, Maire V, Prentice IC, Westoby M, Díaz S, Gallagher RV,**
746 **Jacobs BF, Kooyman R, Law EA et al. 2017.** Global climatic drivers of leaf
747 size. *Science* **357**: 917-921.

748

749 **Figure legends**

750 Fig. 1 Geographical and climatic coverage of the trait dataset. The individual sites are
751 shown as red dots superimposed on a simplified vegetation map of China in (a); these
752 sites have been grouped into eight named regions. The distribution of sites in climate
753 space is shown in (b), where MI is the moisture index defined as the ratio of mean
754 annual precipitation to annual equilibrium evapotranspiration, PAR_0 is the
755 accumulated photosynthetically active radiation during the thermal growing season,
756 and the daily mean temperature during the thermal growing season ($mGDD_0$) is shown
757 by the colour of the dots. The grey shading indicates the frequency of different climates,
758 as defined by MI and PAR_0 , in eastern China as a whole.

759 Fig. 2 Trait dimensions from principal component analysis: grey circles are species-site
760 combinations. The traits are LA: leaf area, SLA: specific leaf area, LDMC: leaf dry
761 matter content, N_{area} : leaf nitrogen per unit area, V_{cmax25} : maximum carboxylation rate
762 standardized to 25°C, J_{max25} : maximum electron transport rate standardized to 25°C,
763 and χ : the ratio of intercellular to ambient CO₂ concentration. The four axes of
764 variability related to LA, χ , the leaf economic spectrum and the photosynthetic traits are
765 shown by coloured ellipses on each plot.

766 Fig. 3 Climate-related trait dimensions from redundancy analysis: grey circles are
767 species-site combinations and coloured dots signify named regions as defined in Fig. 1.
768 The traits are: LA: leaf area, SLA: specific leaf area, LDMC: leaf dry matter content,
769 N_{area} : leaf nitrogen per unit area, V_{cmax25} : maximum carboxylation rate standardized to
770 25°C, J_{max25} : maximum electron transport rate standardized to 25°C, and χ : the ratio of
771 intercellular to ambient CO₂ concentration. The climate variables are the ratio of mean
772 annual precipitation to annual equilibrium evapotranspiration (MI), the accumulated
773 photosynthetically active radiation during the thermal growing season (PAR_0) and the
774 daily mean temperature during the thermal growing season ($mGDD_0$).

775 Fig. 4 Residual (climate-independent) dimensions of trait variation: grey circles are
776 species-site combinations. The traits are: LA: leaf area, SLA: specific leaf area, LDMC:
777 leaf dry matter content, N_{area} : leaf nitrogen per unit area, V_{cmax25} : maximum
778 carboxylation rate standardized to 25°C, J_{max25} : maximum electron transport rate
779 standardized to 25°C, and χ : the ratio of intercellular to ambient CO₂ concentration.

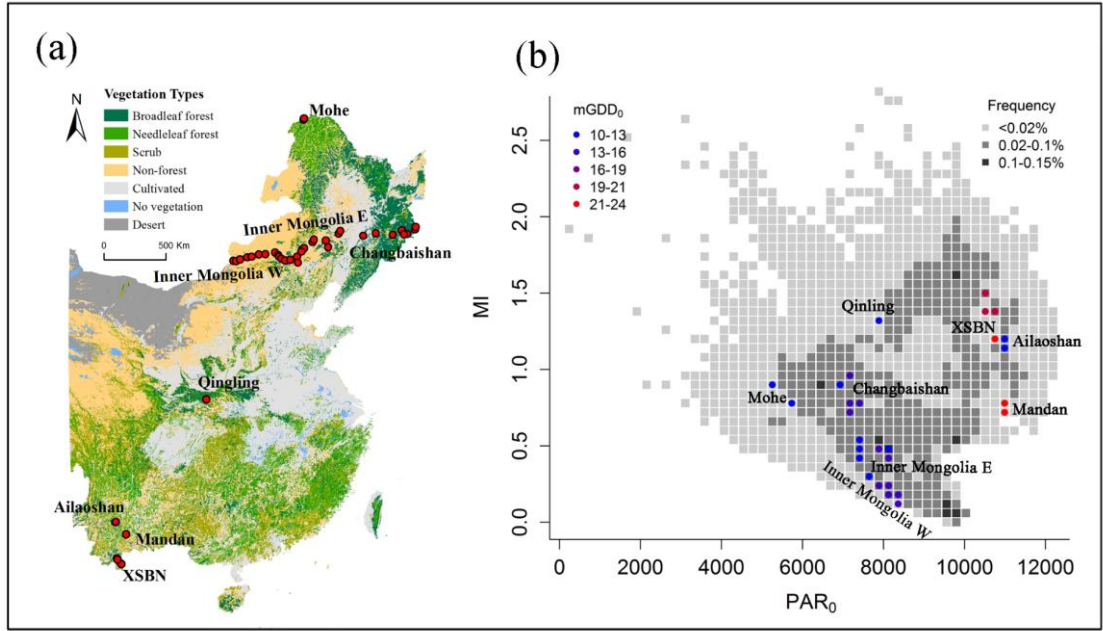
780 Fig. 5 Partial correlations between traits, after removal of climate effects. The traits are:
781 LA: leaf area, SLA: specific leaf area, LDMC: leaf dry matter content, N_{area} : leaf
782 nitrogen per unit area, V_{cmax25} : maximum carboxylation rate standardized to 25°C,
783 J_{max25} : maximum electron transport rate standardized to 25°C, and χ : the ratio of
784 intercellular to ambient CO₂ concentration. Colours indicate the strength of the
785 correlation, where dark blue indicates perfect correlation.

786 Fig. 6 Variance partitioning (%) for all traits considered together, and each trait
787 separately. The traits are: LA: leaf area, SLA: specific leaf area, LDMC: leaf dry matter
788 content, N_{area} : leaf nitrogen per unit area, V_{cmax25} : maximum carboxylation rate
789 standardized to 25°C, J_{max25} : maximum electron transport rate standardized to 25°C,
790 and χ : the ratio of intercellular to ambient CO₂ concentration.

791 Fig. 7 Predicting traits globally at site level, from the trait-climate relationships derived
792 from data in China. The traits are: LA: leaf area, SLA: specific leaf area, LDMC: leaf
793 dry matter content, N_{area} : leaf nitrogen per unit area, V_{cmax25} : maximum carboxylation
794 rate standardized to 25°C, J_{max25} : maximum electron transport rate standardized to
795 25°C, and χ : the ratio of intercellular to ambient CO₂ concentration. (a) Predicted
796 $\ln\sqrt{\text{LA}}$ versus observed $\ln\sqrt{\text{LA}}$ (Wright et al., 2017). (b) Predicted $\ln \text{SLA}$ versus
797 observed $\ln \text{SLA}$ (Wright et al., 2004). (c) Predicted $\ln \text{LDMC}$ versus observed \ln
798 LDMC (Wright et al., 2004). (d) Predicted $\ln N_{\text{area}}$ versus observed $\ln N_{\text{area}}$ (Wright et al.,
799 2004). (e) Predicted $\ln V_{\text{cmax25}}$ versus observed $\ln V_{\text{cmax25}}$ (De Kauwe et al., 2016). (f)
800 Predicted $\ln J_{\text{max25}}$ versus observed $\ln J_{\text{max25}}$ (De Kauwe et al., 2016). (g) Predicted logit
801 χ versus observed logit χ (Cornwell et al., 2017). Red squares are site means.

Figures

Fig.1 Geographical and climatic coverage of the trait dataset. The individual sites are shown as red dots superimposed on a simplified vegetation map of China in (a); these sites have been grouped into eight named regions. The distribution of sites in climate space is shown in (b), where MI is the moisture index defined as the ratio of mean annual precipitation to annual equilibrium evapotranspiration, PAR_0 is the accumulated photosynthetically active radiation during the thermal growing season, and the daily mean temperature during the thermal growing season ($mGDD_0$) is shown by the colour of the dots. The grey shading indicates the frequency of different climates, as defined by MI and PAR_0 , in eastern China as a whole.



813 Fig. 2 Trait dimensions from principal component analysis: grey circles are species-site
814 combinations. The traits are LA: leaf area, SLA: specific leaf area, LDMC: leaf dry
815 matter content, N_{area} : leaf nitrogen per unit area, V_{cmax25} : maximum carboxylation rate
816 standardized to 25°C, J_{max25} : maximum electron transport rate standardized to 25°C,
817 and χ : the ratio of intercellular to ambient CO₂ concentration. The four axes of
818 variability related to LA, χ , the leaf economic spectrum and the photosynthetic traits are
819 shown by coloured ellipses on each plot.

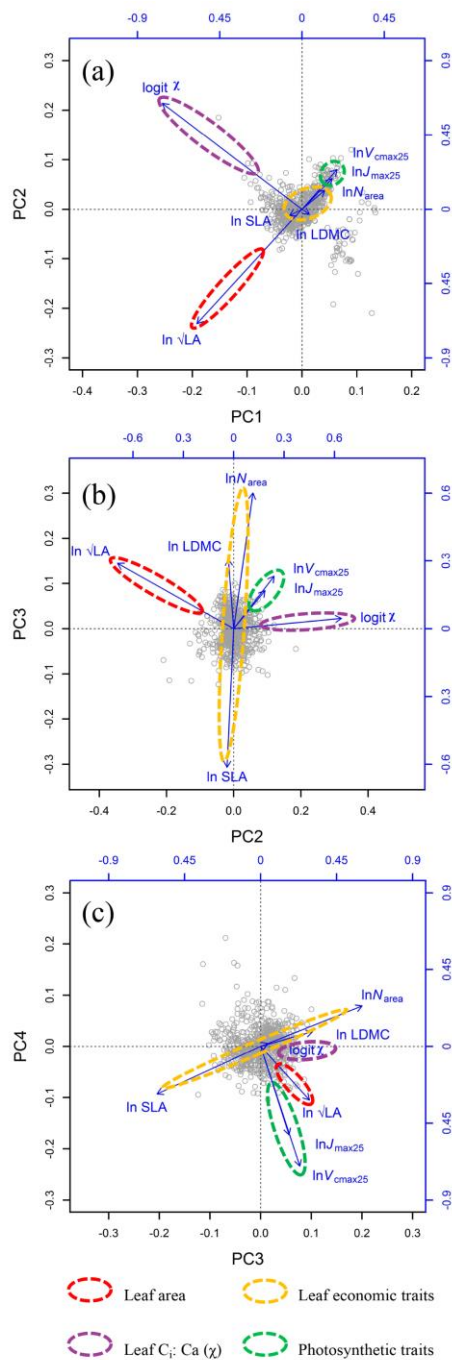
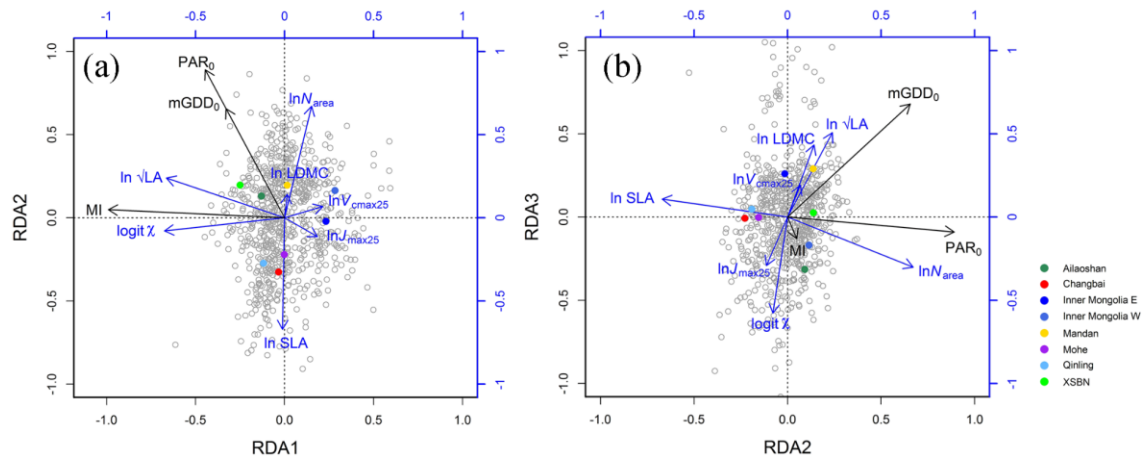


Fig. 3 Climate-related trait dimensions from redundancy analysis: grey circles are species-site combinations and coloured dots signify named regions as defined in Fig. 1. The traits are: LA: leaf area, SLA: specific leaf area, LDMC: leaf dry matter content, N_{area} : leaf nitrogen per unit area, V_{cmax25} : maximum carboxylation rate standardized to 25°C, J_{max25} : maximum electron transport rate standardized to 25°C, and χ : the ratio of intercellular to ambient CO₂ concentration. The climate variables are the ratio of mean annual precipitation to annual equilibrium evapotranspiration (MI), the accumulated photosynthetically active radiation during the thermal growing season (PAR₀) and the daily mean temperature during the thermal growing season (mGDD₀).



829 Fig. 4 Residual (climate-independent) dimensions of trait variation: grey circles are
830 species-site combinations. The traits are: LA: leaf area, SLA: specific leaf area, LDMC:
831 leaf dry matter content, N_{area} : leaf nitrogen per unit area, V_{cmax25} : maximum
832 carboxylation rate standardized to 25°C, J_{max25} : maximum electron transport rate
833 standardized to 25°C, and χ : the ratio of intercellular to ambient CO₂ concentration.

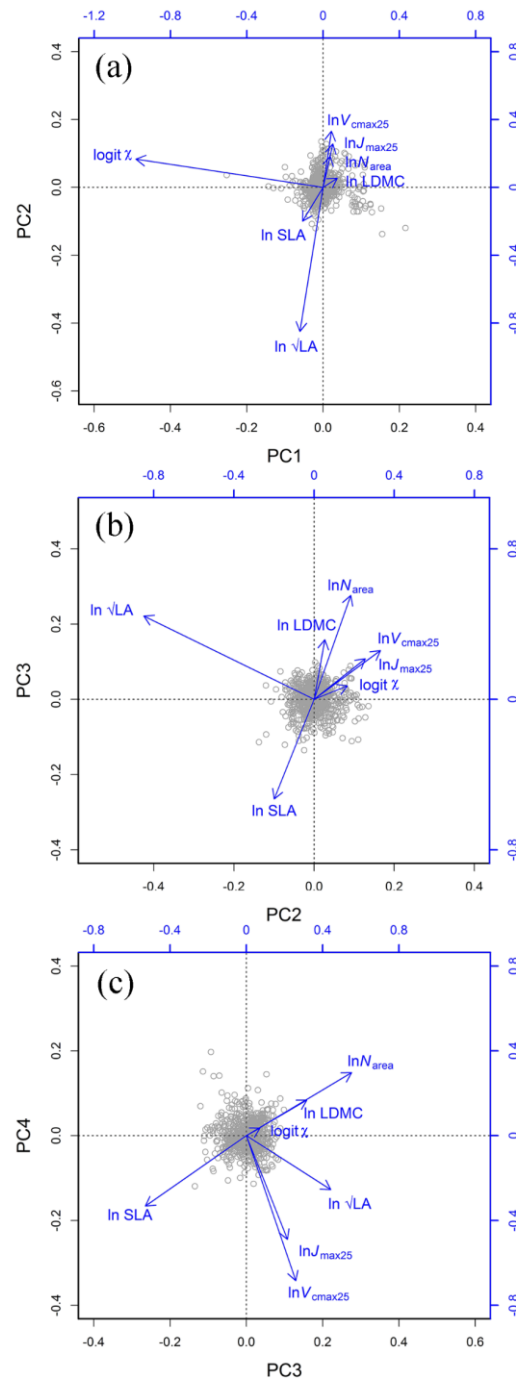
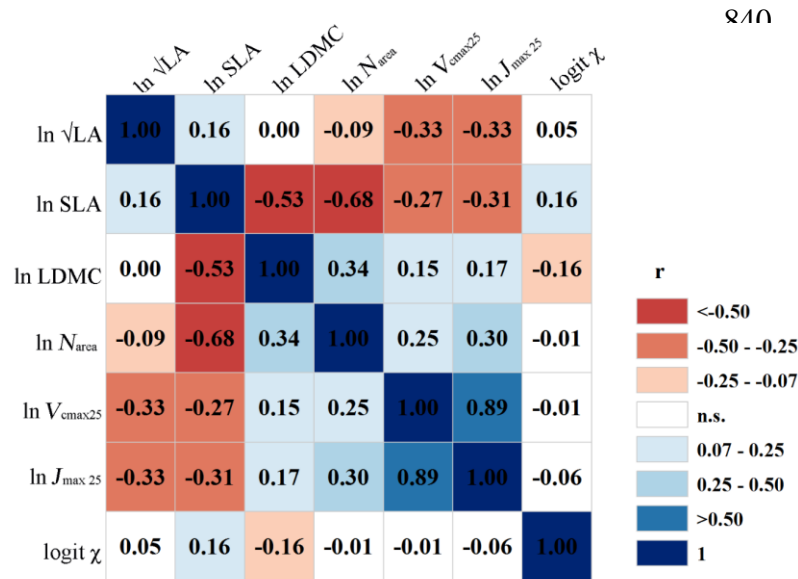


Fig. 5 Partial correlations between traits after removal of climate effects. The traits are:
 LA: leaf area, SLA: specific leaf area, LDMC: leaf dry matter content, N_{area} : leaf
 nitrogen per unit area, $V_{\text{cmax}25}$: maximum carboxylation rate standardized to 25°C,
 $J_{\text{max}25}$: maximum electron transport rate standardized to 25°C, and χ : the ratio of
 intercellular to ambient CO₂ concentration. Colours indicate the strength of the
 correlation, where dark blue indicates perfect correlation.



841 Fig. 6 Variance partitioning (%) for all traits considered together, and each trait
842 separately. The traits are: LA: leaf area, SLA: specific leaf area, LDMC: leaf dry matter
843 content, N_{area} : leaf nitrogen per unit area, V_{cmax25} : maximum carboxylation rate
844 standardized at 25°C, J_{max25} : maximum electron transport rate standardized at 25°C, and
845 χ : the ratio of intercellular to ambient CO₂ concentration.

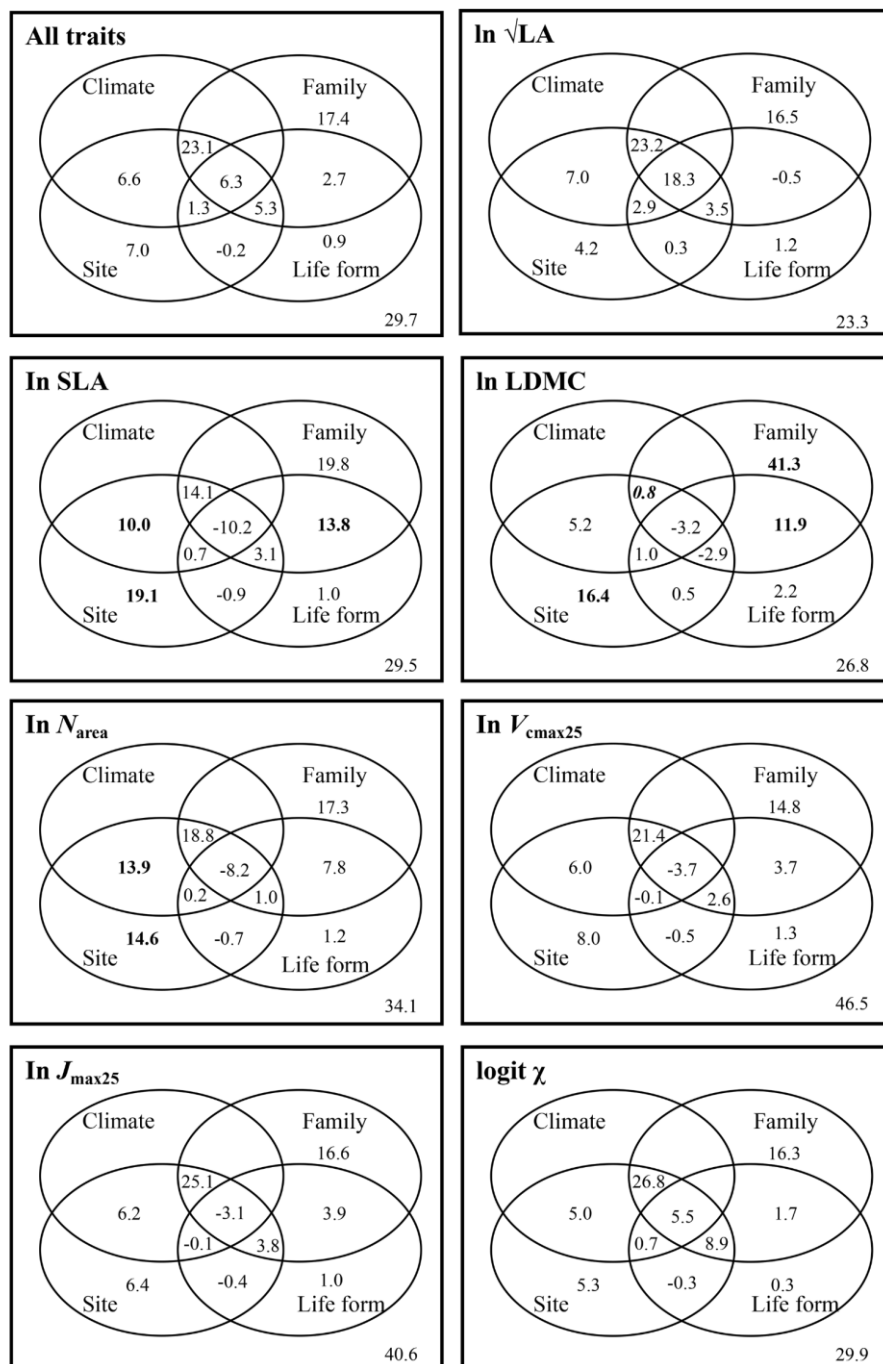
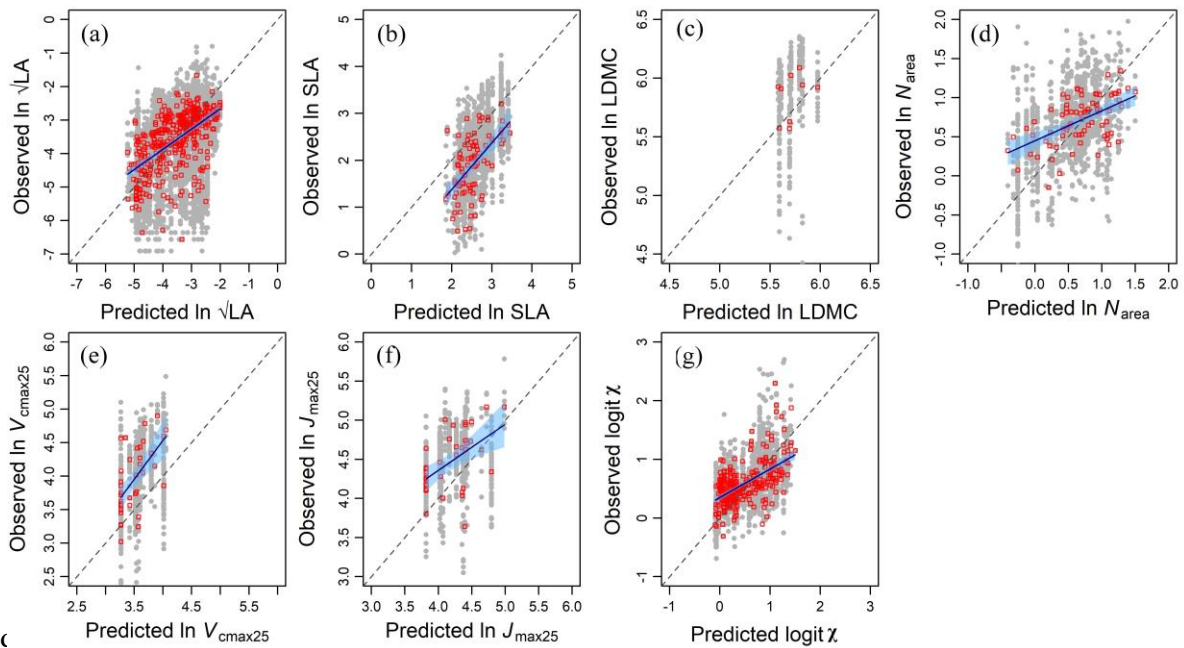


Fig. 7 Predicting traits globally at site level, from the trait-climate relationships derived from data in China. The traits are: LA: leaf area, SLA: specific leaf area, LDMC: leaf dry matter content, N_{area} : leaf nitrogen per unit area, V_{cmax25} : maximum carboxylation rate standardized to 25°C, J_{max25} : maximum electron transport rate standardized to 25°C, and χ : the ratio of intercellular to ambient CO₂ concentration. (a) Predicted $\ln\sqrt{\text{LA}}$ versus observed $\ln\sqrt{\text{LA}}$ (Wright et al., 2017). (b) Predicted $\ln \text{SLA}$ versus observed $\ln \text{SLA}$ (Wright et al., 2004). (c) Predicted $\ln \text{LDMC}$ versus observed $\ln \text{LDMC}$ (Wright et al., 2004). (d) Predicted $\ln N_{\text{area}}$ versus observed $\ln N_{\text{area}}$ (Wright et al., 2004). (e) Predicted $\ln V_{\text{cmax25}}$ versus observed $\ln V_{\text{cmax25}}$ (De Kauwe et al., 2016). (f) Predicted $\ln J_{\text{max25}}$ versus observed $\ln J_{\text{max25}}$ (De Kauwe et al., 2016). (g) Predicted $\text{logit } \chi$ versus observed $\text{logit } \chi$ (Cornwell et al., 2017). Red squares are site means.



861 Table 1 Trait loadings, eigenvalues, and the percentage of trait variation explained by
862 successive principal components in the trait PCA. Loadings > 0.3 in magnitude are
863 shown in **bold**.

	PC1	PC2	PC3	PC4
$\ln \sqrt{\text{LA}}$	-0.57	-0.69	0.29	-0.31
$\ln \text{SLA}$	-0.07	-0.04	-0.61	-0.28
$\ln \text{LDMC}$	0.04	-0.03	0.31	0.09
$\ln N_{\text{area}}$	0.12	0.11	0.60	0.24
$\ln V_{\text{cmax},25}$	0.19	0.24	0.23	-0.70
$\ln J_{\text{max},25}$	0.16	0.19	0.17	-0.52
$\text{logit } \chi$	-0.76	0.64	0.05	0.02
Eigenvalue	2.57	0.90	0.50	0.25
Explained (%)	58.0	20.4	11.3	5.6
Cumulative (%)	58.0	78.5	89.8	95.4

864

865 Table 2 Trait loadings, eigenvalues, and the percentage of trait variation explained by
866 successive RDA axes (constrained by climate) and residual principal components, with
867 axes 1 and 2 mirrored to facilitate comparison with the PCA. Loadings > 0.3 in
868 magnitude are shown in **bold**.

	RDA1	RDA2	RDA3	PC1	PC2	PC3	PC4
$\ln \sqrt{\text{LA}}$	-0.66	0.24	0.51	0.12	-0.85	-0.44	0.25
$\ln \text{SLA}$	-0.01	-0.67	0.11	0.11	-0.20	0.53	0.33
$\ln \text{LDMC}$	0.02	0.14	0.43	-0.08	0.05	-0.32	-0.17
$\ln N_{\text{area}}$	0.15	0.67	-0.30	-0.04	0.18	-0.55	-0.30
$\ln V_{\text{cmax},25}$	0.22	0.07	0.19	-0.04	0.33	-0.26	0.68
$\ln J_{\text{max},25}$	0.18	-0.11	-0.29	-0.05	0.26	-0.22	0.49
$\text{logit } \chi$	-0.67	-0.08	-0.58	0.98	0.17	-0.07	-0.04
Eigenvalue	1.55	0.08	0.02	1.19	0.75	0.42	0.24
Explained (%)	34.9	1.8	0.4	26.8	17.0	9.6	5.3
Cumulative (%)	34.9	36.7	37.1	63.9	80.9	90.5	95.9

869

870 Table 3 Total contributions (%) of climate, family, site and life form to trait variation.
871 Standard deviations (weights) of the transformed variables are also given.

	All traits	$\ln \sqrt{LA}$	$\ln SLA$	$\ln LDMC$	$\ln N_{area}$	$\ln V_{cmax25}$	$\ln J_{max25}$	$\text{logit } \chi$
Weights		1.17	0.50	0.38	0.59	0.58	0.48	1.37
Climate	37.3	51.4	14.6	3.7	24.7	23.6	28.1	38.0
Family	54.8	61.0	40.5	48.0	36.7	38.8	46.3	59.0
Site	49.4	59.4	35.9	17.8	39.6	33.7	37.9	51.8
Life form	16.3	25.8	7.5	9.4	1.3	3.4	5.1	16.7

872

873 Table 4 Prediction accuracy of the trait-climate RDA model for independent global data
874 sets at site level. * indicates that the slope is significantly different from 1 ($P < 0.01$), #
875 indicates that the intercept is significantly different from 0 ($P < 0.01$). ** indicates that
876 the regression is significant ($P < 0.01$).

Traits	Slope	Intercept	R^2_{adj}	n	RMSE	Source of data
$\ln \sqrt{LA}$	0.60* (0.52, 0.70)	-1.45# (-1.72, -1.10)	0.34**	388	0.70	Wright et al. (2017)
$\ln SLA$	0.99 (0.68, 1.31)	-0.61 (-1.41, 0.19)	0.31**	87	0.53	Wright et al. (2004)
$\ln LDMC$	n.s.	n.s.	0.01	9	0.20	Wright et al. (2004)
$\ln N_{area}$	0.38* (0.24, 0.52)	0.45# (0.34, 0.56)	0.28**	77	0.26	Wright et al. (2004)
$\ln V_{cmax25}$	1.16 (0.62, 1.69)	-0.11 (-1.97, 1.76)	0.33**	38	0.40	De Kauwe et al. (2016)
$\ln J_{max25}$	0.59* (0.27, 0.92)	1.99# (0.62, 3.36)	0.25**	38	0.33	De Kauwe et al. (2016)
$\text{logit } \chi$	0.48* (0.40, 0.57)	0.35# (0.30, 0.40)	0.33**	281	0.29	Cornwell et al. (2017)